



Semi-analytical investigation on a mixed boundary value problem in Magnetohydrodynamic fluid flow

Ponpandi Muthumeena and Vembu Ananthaswamy*

Research Scholar, Research Centre and PG Department of Mathematics, The Madura College (Affiliated to Madurai Kamaraj University), Madurai, Tamil Nadu, India.

Abstract

This study looks into magneto-radiative Williamson nanofluid flow with entropy generation in a Darcy-Forchheimer porous medium, incorporating motile microorganisms, activation energy, Brownian motion, thermophoresis, and chemical reactions. Solutions for non-linear differential equations are obtained semi-analytically using the Homotopy Analysis Method (HAM) and Modified Homotopy Analysis Method (MHAM), with results validated through numerical results. Notable discoveries include increased velocity profiles with magnetic field and Darcy-Forchheimer number, enhanced entropy generation with Brinkman number and magnetic field and reduced motile microorganism profiles with bioconvection Lewis number and Peclet number, refining comprehension of thermal interactions and cooling mechanisms using nanofluids. The HAM approach yields semi-analytical outcomes in a direct manner and explicit form, and its appropriateness is adaptable for solving complex non-linear problems in physics, chemistry as well as biology. Furthermore, by comparing numerical values of published works with mathematical expressions for the skin friction coefficient, Sherwood number, Nusselt number and motile microorganism density number are developed also validated, providing high consistency in confirming the validity of the analytical approximations results.

Keywords. Bioconvection, Darcy-Forchheimer, Entropy generation, Motile microorganisms, Thermal radiation, Modified homotopy analysis method (MHAM).

2010 Mathematics Subject Classification. 34B60,34E05,34E10,34E20.

1. INTRODUCTION

A novel development in fluid dynamics, nanofluids are made up of nanoparticles scattered all over regular fluids to improve thermal conductivity. By strategically managing the consistency and distribution of nanoscale particle. In 1995, Choi and Eastman [16] from National laboratory located in Argonne first presented the view of nanofluids. Later studies by Adnan et al. [4] showed that, in comparison to those with only nano-dimensions, nanofluids with silver nanostructures have improved thermal transfer efficiency. The thermodynamic characteristics of second-grade nanofluid flow along a stretching sheet were inspected by Paul et al. [32], taking chemical reactions as well as radiation into account. Magnetohydrodynamic(MHD) hybrid nanofluid transport in porous materials over a vertical stretching surface of a cylinder with heat stratification effects was investigated by Ahmed et al. [1] and for circular channel by Sharma et.al [34]. The publications of Ali et al. [2] and Asjad et al. [10] contain recent noteworthy studies on nanofluids with a variety of properties. Cao et al. [15] and Akbarov et al. [6], focus on heat transfer in Maxwell nanofluids and hydro-elastic systems. These investigations, along with work by Dawood et al. [17], utilize advanced mathematical methods to gain insights into complex phenomena.

With uses in astrophysics, engineering and geophysics, the magnetohydrodynamic Williamson fluid exhibits non-Newtonian behavior, marked by a power-law stress-strain rate dependency. Activation energy and MHD effects with bioconvection, heat radiation and diffusion in magneto-Williamson and Casson fluid flows, heat and mass transfer

Received: 08 August 2025 ; Accepted: 06 October 2025.

* Corresponding author. Email: ananthu9777@gmail.com.

in MHD Williamson nanofluid flow and heat and mass transport in hydromagnetic Williamson nanofluid dynamics involving suction as well injection, buoyancy, radiation also chemical reaction effects are some of the recent studies that have investigated its dynamics by Awan et al. [3] and Dhlamini et.al [18].

Darcy-Forchheimer flow regime is essential in fluid dynamics, presenting analysis into fluid motion in porous media. It combines Darcy's law with Forchheimer's extension, accounting for non-linear effects like inertial resistance and turbulence. This model is crucial in geosciences, petroleum, environmental engineering and industrial filtration. Researchers have made use of it to study various phenomena, encompassing mixed convective flow with Joule heating by Sharma and Gandhi [35], chemically reacting flow with activation energy, irreversibility analysis of radiative nanofluid flow and MHD flow with viscous dissipation and variable fluid properties. Activation energy is a primary concept in chemical kinetics, referring to the minimum energy required for reactant molecules to overcome the challenge and transform into products. Its applications span cancer treatment, drug formulation and food preservation. Researchers have studied its effects in various nanofluid flows, including magneto-Williamson nanofluid, combined convective nanofluid flow by Dhlamini et al. [19], Prandtl-Eyring nanofluid, and Maxwell flow of fluid across a Riga plate in a porous material by Vijayalakshmi et al. [40], highlighting its significance in chemical reactions and fluid dynamics. Agrwall et al. [5] and Lakestani et al. [23] explores various topics in fluid dynamics and mathematical modeling, including micropolar fluid flows and analytical solutions to modified dispersive water-wave systems.

Entropy generation in fluid flow represents the one-way increase in entropy due to dissipative processes, crucial for optimizing system designs and efficiency. Its applications span heat exchange, turbines, and environmental remediation. Researchers have studied entropy generation in various fluid flows, including MHD radiative transport of Williamson nanofluid by Kumar et al. [21], Kumaran and Sandeep [22], viscous flow over a stretching cylinder by Butt et al. [14], magneto-viscoelastic flow by Baag et al. [13], radiative nanomaterial flow, magneto-nanofluid boundary layer flow by Ullah et al. [39], and bio-convective micropolar nanofluid flow, highlighting its significance in thermodynamic analysis and optimization. Recent studies have explored the dynamics of gyrotactic microorganisms in various fluid flows. Haq et al. [20] investigated the behavior of gyrotactic microorganisms in radiated nanomaterial Williamson fluid with activation energy. Song et al. [36] analyzed the bidirectional nonlinear stretched flow of Williamson nanofluid with motile gyrotactic microorganisms. These studies highlight the significance of microorganisms in fluid dynamics and their potential applications.

This study investigates magneto-Darcy Forchheimer flow of bioconvective Williamson nano scale fluid along a stretching sheet, focusing on entropy generation, activation energy also motile microorganisms. Incorporating thermal radiation, suction/injection and heat source effects, this research provides a novel approach to understanding complex phenomena. Utilising the HAM and MHAM, semi-analytical answers for density, temperature, velocity and concentration are obtained. Semi-analytical mathematical solutions are expressed for motile density number, skin friction coefficient, Sherwood number, and Nusselt number. These results are compared with numerical solutions using tables. Additionally, graphical representations of the previously described functions, constants, and entropy generation are also presented.

2. MATHEMATICAL FORMULATION OF THE PROBLEM

The present work examines the mathematical modeling of entropy optimization in Williamson nanofluid flow, considering factors like magneto-Darcy Forchheimer flow, motile microorganisms, Brownian motion, thermophoresis, radiation, heat sources, chemical reactions and activation energy. Figure [1] illustrates the flow configuration for the current model. Boundary sheet of the flow dynamics issue is susceptible to flow in the x -direction, with the y -direction perpendicular to it. The linear velocity of the stretching sheet is assumed to be $u_w = ax$, with uniform thermal and concentration conditions T_w and C_w while ambient concentration(C_∞) also temperature(T_∞). The controlling equations for flow are detailed in the work of Kumar et al. [21], Reddy et al. [33] and Butt et al. [14].

$$\frac{\partial u}{\partial x} + \frac{\partial v}{\partial y} = 0, \quad (2.1)$$

$$u \frac{\partial u}{\partial x} + v \frac{\partial u}{\partial y} = v \frac{\partial^2 u}{\partial y^2} + \sqrt{2}v\Gamma \frac{\partial u}{\partial y} \frac{\partial^2 u}{\partial y^2} - \frac{\sigma B_0^2 u}{\rho} - \frac{\mu}{\rho k_1} u - \frac{c_b}{\sqrt{k_1}} u^2, \quad (2.2)$$



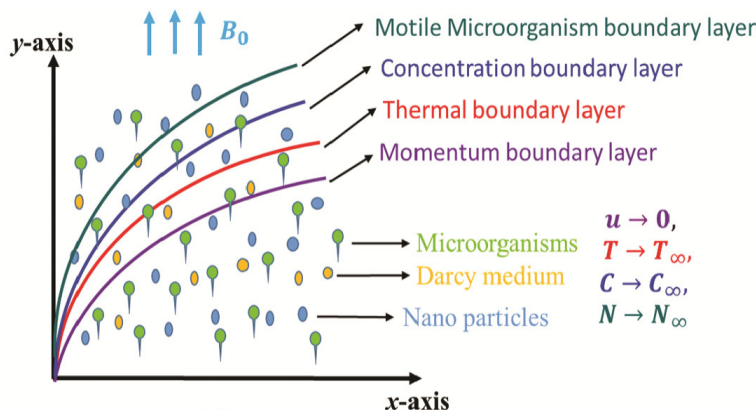


FIGURE 1. Illustration of the flow geometry.

$$u \frac{\partial T}{\partial x} + v \frac{\partial T}{\partial y} = \left(\frac{\mu}{\rho C_P} \right) \left(\frac{\partial u}{\partial y} \right)^2 + \left(\frac{\mu}{\rho C_P} \right) \Gamma \left(\frac{\partial u}{\partial y} \right)^3 + \tau \left(D_B \frac{\partial c}{\partial y} \frac{\partial T}{\partial y} + \frac{D_T}{T_\infty} \left(\frac{\partial T}{\partial y} \right)^2 \right) + \alpha \frac{\partial^2 T}{\partial y^2} - \frac{1}{\rho C_P} \frac{\partial q_r}{\partial y} + \frac{Q_0}{\rho C_P} (T - T_\infty) + \frac{\sigma \beta_0^2}{\rho C_P} u^2, \tag{2.3}$$

$$u \frac{\partial C}{\partial x} + v \frac{\partial C}{\partial y} = D_B \frac{\partial^2 C}{\partial y^2} + \frac{D_T}{T_\infty} \frac{\partial^2 T}{\partial y^2} - K_r^2 (C - C_\infty) \left(\frac{T}{T_\infty} \right)^n \exp \left(\frac{-E_a}{kT} \right), \tag{2.4}$$

$$\left(u \frac{\partial N}{\partial x} + v \frac{\partial N}{\partial y} \right) = D_m \frac{\partial^2 N}{\partial y^2} + \frac{b w_c}{(C_w - C_\infty)} \frac{\partial}{\partial y} \left(N \frac{\partial C}{\partial y} \right). \tag{2.5}$$

The specified boundary value conditions are listed below:

$$\begin{aligned} \text{At } y = 0: & \quad u = u_w, v = v_w, \frac{\partial T}{\partial y} = \frac{-h_f}{k} (T_w - T), C = C_w, N = N_w, \\ \text{As } y \rightarrow \infty: & \quad u \rightarrow 0, T \rightarrow T_\infty, C \rightarrow C_\infty, N \rightarrow N_\infty. \end{aligned} \tag{2.6}$$

The governing equations are reduced through the similarity transformations: ([17],[12])

$$\begin{aligned} u = ax f'(\eta), v = -\sqrt{av} f(\eta), \eta = \sqrt{\frac{a}{\nu}} y, \theta(\eta)(T_w - T_\infty) = T - T_\infty, \\ \phi(\eta)(C_w - C_\infty) = C - C_\infty, \chi(\eta)(N_w - N_\infty) = N - N_\infty. \end{aligned} \tag{2.7}$$

Using similarity transformations in Eqs. (2.2)–(2.6) formulated to

$$(1 + We f'') f''' - (M + K) f' + f f'' - Fr f'^2 - f'^2 = 0, \tag{2.8}$$

$$\left(1 + \frac{4}{3} R \right) \theta'' + Pr \left[f \theta' + Nb \theta' \phi' + Nt \theta'^2 + MEc f'^2 + Ec f''^2 + \frac{1}{\sqrt{2}} Ec We f''^3 + Q\theta \right] = 0, \tag{2.9}$$

$$\phi'' + Sc f \phi' + \left(\frac{Nt}{Nb} \right) \theta'' - Sc Cr (1 + \alpha_1 \theta)^n \exp \left(\frac{-E}{1 + \alpha_1 \theta} \right) \phi = 0, \tag{2.10}$$

$$\chi'' + Lb f \chi' - Pe [(\delta_1 + \chi) \phi'' + \chi' \phi'] = 0. \tag{2.11}$$

The conditions at the boundary are:

$$\begin{aligned} f(0) = S, \quad f'(0) = 1, \quad \theta'(0) = Bi(\theta(0) - 1), \quad \phi(0) = 1, \quad \chi(0) = 1, \\ f'(\infty) = 0, \quad \theta(\infty) = 0, \quad \phi(\infty) = 0, \quad \chi(\infty) = 0, \end{aligned} \tag{2.12}$$



where

$$\begin{aligned}
M &= \frac{\sigma B_o^2}{\rho a}, & K &= \frac{v}{ak_1}, & We &= \Gamma u_w \sqrt{\frac{2a}{v}}, & Fr &= \frac{c_b}{\sqrt{k_1}}, \\
Pr &= \frac{v}{\alpha}, & Q &= \frac{Q_o}{\rho C_p a}, & Ec &= \frac{u_w^2}{(T_w - T_\infty) C_p}, & Nb &= \frac{\tau D_B (C_w - C_\infty)}{v}, \\
Lb &= \frac{v}{D_m}, & S &= -\frac{v_w}{\sqrt{av}}, & Bi &= \frac{h_f}{k} \sqrt{\frac{v}{a}}, & Sc &= \frac{v}{D_B}, \\
R &= \frac{4\sigma^* T_\infty^3}{k^* k}, & Nt &= \frac{\tau D_T (T_w - T_\infty)}{T_\infty v}, & Cr &= \frac{K_r}{a}.
\end{aligned} \tag{2.13}$$

The skin friction, Motile density number, Sherwood number also Nusselt number outlined below:

$$\sqrt{\text{Re}_x} C_f = \left(1 + \frac{We}{2}\right) f''(0), \quad \frac{Nh}{\sqrt{\text{Re}_x}} = -\chi'(0), \quad \frac{Sh}{\sqrt{\text{Re}_x}} = -\phi'(0), \quad \frac{Nu}{\sqrt{\text{Re}_x}} = -\left(1 + \frac{4}{3}R\right) \theta'(0), \tag{2.14}$$

2.1. Investigation of entropy generation. Magneto-Williamson nano scale fluid's volumetric entropy generation is represented as:

$$\begin{aligned}
Ns &= \alpha_1 \left(1 + \frac{4}{3}R\right) \theta'^2 + Br \left(f''^2 + \frac{We}{\sqrt{2}} f''^3\right) + L_1 \left(\frac{\alpha_2}{\alpha_1}\right) \phi'^2 \\
&+ Br(M + K)F'^2 + L_1 \theta' \phi' + L_2 \left(\frac{\alpha_3}{\alpha_1}\right) \chi'^2 + L_2 \chi' \theta',
\end{aligned} \tag{2.15}$$

such that,

$$\begin{aligned}
Br &= \frac{\mu_o u_w^2}{k \Delta T}, \quad L_1 = \frac{RD(C_w - C_\infty)}{k}, \quad L_2 = \frac{RD(N_w - N_\infty)}{k}, \\
We &= \Gamma u_w \sqrt{\frac{2a}{v}}, \quad \alpha_2 = \frac{\Delta C}{C_\infty}, \quad \alpha_1 = \frac{\Delta T}{T_\infty}, \quad \alpha_3 = \frac{\Delta N}{N_\infty},
\end{aligned} \tag{2.16}$$

correspond to Brinkman number, diffusion parameter due to concentration, diffusion parameter due to microorganisms, Williamson fluid, concentration difference parameter, concentration difference of microorganisms additionally temperature difference parameter.

3. SEMI-ANALYTICAL EXPRESSION OF NON-LINEAR BOUNDARY VALUE PROBLEM THROUGH HAM AND MHAM

The Homotopy analysis method (HAM) is a powerful, analytical technique for solving non-linear differential equations, facilitating adaptable convergence through a convergence-control parameter. Successfully applied across various scientific and engineering disciplines, HAM excels in handling highly non-linear differential equations. We utilize HAM to investigate MHD flow problems, providing solutions as infinite power series that require numerical evaluation for practical applications. With an auxiliary parameter, HAM allows control over convergence regions, making it superior to other perturbation methods. Proposed by Liao ([25–31]), HAM's flexibility and effectiveness make it an ideal choice for tackling complex nonlinearities in MHD flow and similar problems as also demonstrated by Ananthaswamy et al. ([8–11, 38])

The Modified Homotopy analysis method (MHAM) ([7, 24, 37]) further enhances this versatility, applicable to both linear and non-linear types of differential equations. MHAM addresses various non-linear boundary value problems(bvp) in physics, chemistry and biology, particularly in MHD flow problems. Key advantages of MHAM include simplicity, rapid convergence typically within a single iteration, and high accuracy with error percentages below 0.3% compared to numerical solutions. The solution involves arbitrary constants dependent on the differential equation's order, facilitating determination and application. By leveraging MHAM's strengths, researchers can efficiently obtain accurate analytical solutions for complex non-linear bvps. MHAM's effectiveness and efficiency provide a powerful



resource for scientists as well as researchers tackling challenging problems, offering reliable results with minimal computational effort. The outcomes computed for the unit less velocity, concentration, density distributions and temperature are outlined below, accompanied by their approximate analytical formulations.

3.1. Semi-analytical outcomes of velocity distribution using HAM ([28–31]): A semi-analytical solution is presented below for the velocity profile in Eq. (2.8) subject to the boundary specifications (2.12).

$$f(\eta) = S + \frac{1}{\sqrt{M+K}} - \frac{e^{-\sqrt{M+K}\eta}}{\sqrt{M+K}} + h \left[\begin{aligned} & \frac{1}{6} \cdot \frac{We\sqrt[3]{M+K} + 7Fr}{\sqrt[3]{M+K}} + \frac{1}{2} \cdot \frac{1 + 10S\sqrt{M+K}}{\sqrt[3]{M+K}} \\ & + \left(-\frac{1}{2} \cdot \frac{1 + 10S\sqrt{M+K}}{\sqrt[3]{M+K}} - \frac{1}{3} \cdot \frac{We\sqrt[3]{M+K} + 7Fr}{\sqrt[3]{M+K}} \right) e^{-\sqrt{M+K}\eta} \\ & - \frac{1}{2} \cdot \frac{1 + 10S\sqrt{M+K}}{M+K} \cdot \eta e^{-\sqrt{M+K}\eta} \\ & + \frac{1}{6} \cdot \frac{(We\sqrt[3]{M+K} + 7Fr) e^{-2\sqrt{M+K}\eta}}{\sqrt[3]{M+K}} \end{aligned} \right], \tag{3.1}$$

$$f'(\eta) = e^{-\sqrt{M+K}\eta} \left(1 + \frac{1}{3}h \cdot \frac{We(M+K)^{3/2} - 7Fr}{M+K} + h(1 - 10S\sqrt{M+K})\sqrt{M+K} \cdot \eta \right) - \frac{1}{3(M+K)}h \left(We(M+K)^{3/2} - 7Fr \right) e^{-2\sqrt{M+K}\eta}. \tag{3.2}$$

Using the Modified Homotopy analysis method (MHAM), we extract semi-analytical solutions of the transformed temperature, concentration, and density distribution Eqs. (2.9)-(2.11), which fulfills the boundary conditions in Eq. (2.12), as follows:([7, 24])

$$\theta(\eta) = \frac{Bi \times e^{(-A\eta)}}{A + Bi} + h \left[\begin{aligned} & \frac{(MEcR + Nb + Nt)e^{(-A\eta)} PrBiC}{(Q + S)(A + Bi) \left(1 + \frac{4}{3}R\right)} \\ & - \frac{1}{4} \frac{e^{(-2\sqrt{M+K}\eta)} PrEc(2M + K)}{(M + K) \left(1 + \frac{4}{3}R\right)} \\ & - \frac{e^{(-(A+\sqrt{M+K})\eta)} PrBiA}{(A + \sqrt{M + K})^2(A + Bi) \left(1 + \frac{4}{3}R\right) \sqrt{M + K}} \\ & + \frac{1}{18} \frac{\sqrt{M + K} e^{(-3\sqrt{M+K}\eta)} PrEcWe\sqrt{2}}{\left(1 + \frac{4}{3}R\right)} \\ & - \frac{1}{4} \frac{e^{(-2A\eta)} PrNtBi^2}{(A + Bi)^2 \left(1 + \frac{4}{3}R\right)} + \frac{e^{(-(A+B)\eta)} PrNbBiAB}{(A + B)^2(A + Bi) \left(1 + \frac{4}{3}R\right)} \\ & + N_1 - BiN_2 \end{aligned} \right] / Bi, \tag{3.3}$$



$$\phi(\eta) = e^{-B\eta} + h \left[\begin{aligned} & \frac{(E+R)Nt e^{-B\eta} \left(\left(S + \frac{1}{\sqrt{M+K}} \right) ScB + ScCr - ScCrE \right)}{Sc + CrNb} \\ & - \frac{e^{-(\sqrt{M+K}-B)\eta} ScB}{(\sqrt{M+K}+B)^2 \sqrt{M+K}} + \frac{ScB}{(\sqrt{M+K}+B)^2 \sqrt{M+K}} \\ & + \frac{e^{-(A+B)\eta} \left(\frac{ScCrE\alpha_1 Bi + ScCrn\alpha_1 Bi - En\alpha_1 Bi}{A+Bi} \right)}{(A+B)^2} \\ & + \frac{e^{-(2A+B)\eta} n E \alpha_1^2 Bi^2}{(2A+B)^2 (A+Bi)^2} + \frac{Nt Bi}{(A+Bi)Nb} - \frac{e^{-B\eta} Nt Bi}{(A+Bi)Nb} \\ & - \frac{(E+R)Nt \left(\left(S + \frac{1}{\sqrt{M+K}} \right) ScB + ScCr - ScCrE \right)}{Sc + CrNb} \\ & - \left(\frac{ScCrE\alpha_1 Bi + ScCrn\alpha_1 Bi - En\alpha_1 Bi}{(A+Bi)(A+B)^2} \right) \\ & - \frac{n E \alpha_1^2 Bi^2}{(2A+B)^2 (A+Bi)^2} \end{aligned} \right], \quad (3.4)$$

$$\chi(\eta) = e^{(-D\eta)} + h \left[\begin{aligned} & \frac{e^{(-D\eta)} Lb \left(S + \frac{1}{\sqrt{M+K}} \right)}{\sqrt{Lb + Pe\alpha_1}} - \frac{e^{-(\sqrt{M+K}+D)\eta} LbD}{(\sqrt{M+K}+D)^2 \sqrt{M+K}} \\ & - \frac{(E+R)Nt e^{(-B\eta)} Pe\alpha_1}{Sc + CrNb} + \frac{e^{-(B+D)\eta} \left(\frac{Pe(Sc+CrNb)}{(R+E)Nt} - PeDB \right)}{(B+D)^2} \end{aligned} \right], \quad (3.5)$$

where constants which are used in Eqs. (3.1)-(3.5)

$$A = \sqrt{\frac{Q+S}{MEcR + Nb + Nt}}, \quad (3.6)$$

$$B = \sqrt{\frac{Sc + CrNb}{(R+E)Nt}}, \quad (3.7)$$

$$C = \sqrt{\frac{Q+S}{MEcR + Nb + Nt}} \left(S + \frac{1}{\sqrt{M+K}} \right) - Q, \quad (3.8)$$

$$D = \sqrt{Lb + Pe\alpha_1}, \quad (3.9)$$

$$N_1 = \left(\begin{aligned} & \frac{1}{2} \frac{Pr Ec(2M+K)}{\sqrt{M+K} \left(1 + \frac{4}{3}R \right)} - \frac{Pr BiC}{A(A+Bi) \left(1 + \frac{4}{3}R \right)} + \frac{Pr NbABBi}{(A+B)(A+Bi) \left(1 + \frac{4}{3}R \right)} \\ & + \frac{1}{2} \frac{Pr NtBi^2(Q+S)}{A(MEcR + Nb + Nt)(A+Bi)^2 \left(1 + \frac{4}{3}R \right)} - \frac{1}{6} \frac{(M+K) Pr EcW e \sqrt{2}}{\left(1 + \frac{4}{3}R \right)} \\ & + \frac{Pr BiA}{(A + \sqrt{M+K})(A+Bi) \left(1 + \frac{4}{3}R \right) \sqrt{M+K}} \end{aligned} \right), \quad (3.10)$$



$$N_2 = \left(\begin{aligned} & \frac{(MEcR + Nb + Nt) \Pr Bi C}{(Q + S)(A + Bi) \left(1 + \frac{4}{3}R\right)} - \frac{1}{4} \frac{\Pr Ec(2M + K)}{(M + K) \left(1 + \frac{4}{3}R\right)} \\ & - \frac{\Pr Bi A}{(A + \sqrt{M + K})^2 (A + Bi) \left(1 + \frac{4}{3}R\right) \sqrt{M + K}} + \frac{1}{18} \frac{\sqrt{M + K} \Pr Ec We \sqrt{2}}{\left(1 + \frac{4}{3}R\right)} \\ & - \frac{\Pr Nb AB Bi}{(A + B)^2 (A + Bi) \left(1 + \frac{4}{3}R\right)} - \frac{1}{4} \frac{\Pr Nt Bi^2}{(A + Bi)^2 \left(1 + \frac{4}{3}R\right)} \end{aligned} \right). \tag{3.11}$$

3.2. Semi-analytical expression for skin friction coefficient, Nusselt number, motile microorganism density number and Sherwood number. Mathematical formations for skin friction coefficient, Nusselt number, motile microorganism density number and Sherwood number as follows:

$$\sqrt{Re_x} C_f = \left(1 + \frac{We}{2} \right) \left(-\sqrt{M + K} \left(1 + \frac{1}{3} \frac{h(We^3 \sqrt{M + K} - 7Fr)}{M + K} \right) + h(1 - 10S\sqrt{M + K})\sqrt{M + K} + \frac{2}{3} \frac{h(We^3 \sqrt{M + K} - 7Fr)}{\sqrt{M + K}} \right), \tag{3.12}$$

$$\frac{Nu}{\sqrt{Re_x}} = - \left(1 + \frac{4}{3}R \right) \left(\begin{aligned} & - \frac{Bi A}{(A + Bi)} \frac{(MEcR + Nb + Nt) \Pr Bi AC}{(Q + S)(A + Bi) \left(1 + \frac{4}{3}R\right)} \\ & - \frac{\Pr Bi A}{(A + \sqrt{M + K})^2 (A + Bi) \left(1 + \frac{4}{3}R\right) \sqrt{M + K}} \\ & - \frac{\Pr Nb Bi AB}{(A + B)(A + Bi) \left(1 + \frac{4}{3}R\right)} + \frac{1}{2} \frac{\Pr Ec(2M + K)}{(M + K) \left(1 + \frac{4}{3}R\right)} \\ & + \frac{1}{2} \frac{A \Pr Nt Bi^2}{(A + Bi)^2 \left(1 + \frac{4}{3}R\right)} - \frac{1}{6} \frac{(M + K) \Pr Ec We \sqrt{2}}{\left(1 + \frac{4}{3}R\right)} \end{aligned} \right), \tag{3.13}$$

$$\frac{Nh}{\sqrt{Re_x}} = \left(\begin{aligned} & B + Lb \left(S + \frac{1}{\sqrt{M + K}} \right) + \frac{Lb D}{(-\sqrt{M + K} - D)\sqrt{M + K}} \\ & - \frac{B(E + R)Nt Pe \alpha_1}{Sc + Cr Nb} + \frac{\left(\frac{Pe(Sc + Cr Nb)}{(R + E)Nt} - Pe DB \right)}{-(B + D)} \end{aligned} \right), \tag{3.14}$$

$$\frac{Sh}{\sqrt{Re_x}} = \left(\begin{aligned} & \frac{(E + R)Nt B \left(\left(S + \frac{1}{\sqrt{M + K}} \right) Sc B + Sc Cr - Sc Cr E \right)}{Sc + Cr Nb} \\ & + \frac{Sc B}{(\sqrt{M + K} + B)^2 \sqrt{M + K}} - \frac{ANt Bi}{(A + Bi) Nb} \\ & - \frac{\left(\frac{Sc Cr E \alpha_1 Bi + Sc Cr n \alpha_1 Bi - E n \alpha_1 Bi}{A + Bi} \right)}{(A + B)^2} - \frac{n E \alpha_1^2 Bi^2}{(2A + B)^2 (A + Bi)^2} \end{aligned} \right). \tag{3.15}$$

4. RESULTS AND DISCUSSION

The visual portrayal in this segment utilizes the semi-analytical results (via Python 3.10) sketched in Eqs. (3.2)-(3.5), which are compared to numerical results, as shown in Figure 2-18. A high degree of consistency is observed between the semi-analytical and numerical solutions.

The research explores the effects of multiple parameters on velocity as per Eq. (3.2), temperature, concentration and density number as mentioned in Eqs. (3.3)-(3.5). Figures 2-5 indicates velocity profile is influenced by several



factors, including the magnetic field parameter(M), porosity(K), Darcy-Forchheimer (Fr) furthermore suction factor (S), all of which contribute to a diminishes in velocity.

The graphical representations in Figures 6-10 examine how various parameters influence temperature profiles according to Eq. (3.3), such as magnetic parameter (M) in Figure 7, R in Figure 10, Nt in Figure 9 and Nb in Figure 8 which rise up the temperature . However, suction factor (S) has a contrary effect, reducing temperature in Figure 6.

Figures 11-14 present a visual examination of the concentration under the influence of various parameters in line with Eq. (3.4). Brownian motion factor (Nb) in Figure 13 and chemical reaction factor (Cr) in Figure 11 all goes down the concentration. In contrast, and Thermophoresis parameter (Nt) in Figure 14 and energy factor (E) in Figure 12 boost the concentration.

A comprehensive graphical illustration Figures 15 and 16 reveals that Density number of motile microorganisms is influenced by parameters as indicated by Eq. (3.5), while Lb and Pe have a reducing effect.

The relationship between the Brinkman number(Br) and entropy generation is depicted in Figure 17 as per Eq. (2.15), showing a positive correlation. Additionally, Figure 18 illustrates the impact of the M on entropy generation, revealing that a stronger M results in elevated Ns due to enhanced irreversibly.

In Figures 19-22 that an augment in Fr leads to an elevate in magnetic field parameter(M), which in turn affects skin friction in Figure 19. Meanwhile, an grow in Nt results in a diminish in the suction factor(S), impacting the Nusselt number in Figure 20, and an amplifying in E , influence the Sherwood number as Figure 21. Additionally, as Pe rise influencing the motile density number in Figure 22.

Tables 1-4 present the effects of various parameters on skin friction, thermal transmission rate, mass transmission rate as well as motile density number. **Skin friction coefficient** (Table 1) increases with Lorentz force, porosity(K), Forchheimer impact(Fr), and suction velocity(S), but decreases with Williamson fluid factor. **Thermal transmission rate** (Table 2) enhances with suction(S), Pr , R , Q , and Biot number(Bi), while Eckert number(Ec), Brownian motion factor(Nb) additionally Nt exhibit an opposite trend. **Mass transmission rate** (Table 3) increases with Schmidt number(Sc), Cr , and Brownian motion factor(Nb) due to reduced mass diffusivity, accelerated species consumption, and augmented nanoparticle diffusion. Conversely, thermophoresis factor and activation energy(E) decrease mass transport efficiency. **Motile density number** (Table 4) improves with Lb , Pe and δ_1 .

TABLE 1. Comparison of Numerical and Semi-analytical results for $-C_f\sqrt{Re_x}$.

M	K	We	Fr	S	Numerical solution	Semi-analytical solution	Error%
1.0	0.5	0.2	0.5	0.1	1.477742	1.288874	0.146537
2.0	0.5	0.2	0.5	0.1	1.758635	1.635541	0.075262
3.0	0.5	0.2	0.5	0.1	1.996164	1.922485	0.038325
1.0	0.5	0.2	0.5	0.1	1.857811	1.635541	0.135900
1.0	1.0	0.2	0.5	0.1	1.973876	1.802485	0.095086
1.0	1.5	0.2	0.5	0.1	2.082577	1.922485	0.083273
1.0	0.5	0.1	0.5	0.1	1.758635	1.552448	0.132814
1.0	0.5	0.2	0.5	0.1	1.511875	1.635541	0.075612
1.0	0.5	0.3	0.5	0.1	0.97548	1.719467	0.432685
1.0	0.5	0.2	0.5	0.5	1.787103	1.635541	0.092668
1.0	0.5	0.2	1.0	1.0	1.855624	1.647136	0.126576
1.0	0.5	0.2	1.5	0.1	1.920718	1.658731	0.157944
1.0	0.5	0.2	0.5	0.1	1.758635	1.635541	0.075262
1.0	0.5	0.2	0.5	0.2	1.801445	1.641041	0.097745
1.0	0.5	0.2	0.5	0.3	1.845063	1.646541	0.120569
Absolute Average Error Percentage							0.125751



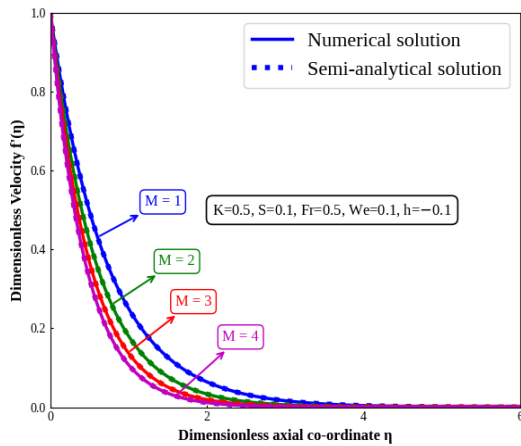


FIGURE 2. Dimensionless velocity versus the non-dimensional axial co-ordinate. The curves are visualized using Eq. (3.2) for selected values of the dimensionless magnetic(M) and the remaining non-dimensional parameters held constant.

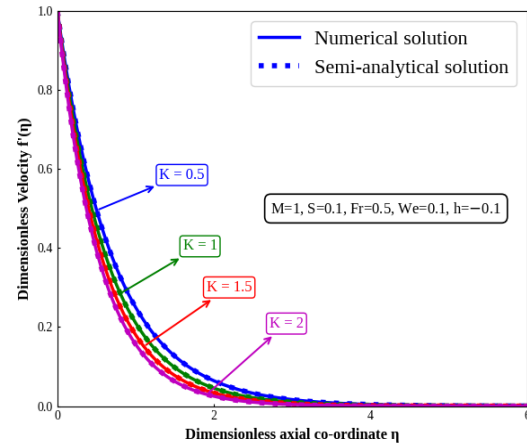


FIGURE 3. Dimensionless velocity in relation to the non-dimensional axial coordinate. For multiple values of dimensionless porosity (K) and holding certain values held constant for other non-dimensional parameters, the curves are plotted using Eq. (3.2).

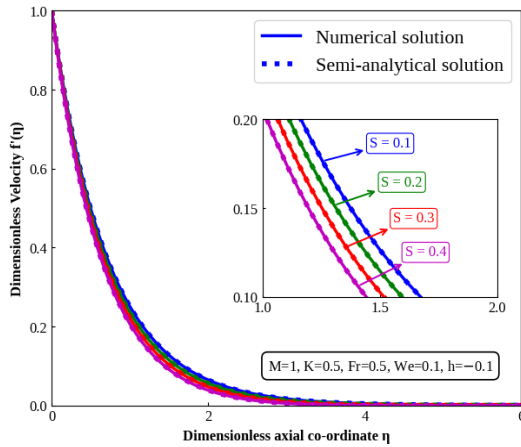


FIGURE 4. Dimensionless velocity against the non-dimensional axial coordinate. The graphs are plotted according to the Eq. (3.2) for several values of the non-dimensional suction factor (S) and in some dimensionless parameters held at fixed values

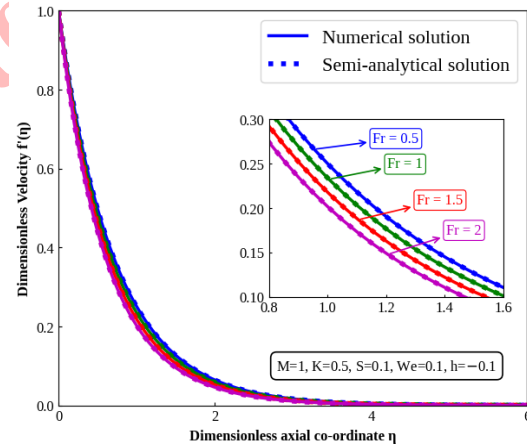


FIGURE 5. Visualization of the non-dimensional velocity versus the dimensionless axial coordinate have been plot using Eq. (3.2) for various values of the non-dimensional Forchheimer inertia factor (Fr), with other dimensionless parameters fixed.

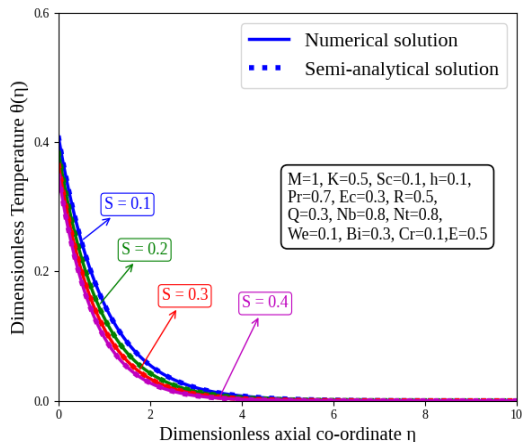


FIGURE 6. Non-dimensional temperature in relation to the non-dimensional axial coordinate. For different values of the dimensionless suction factor (S) and for certain fixed values of further non-dimensional parameters, the curves are plotted using Eq. (3.3).

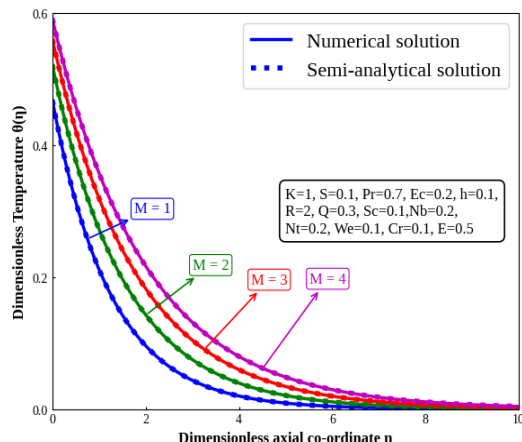


FIGURE 7. Dimensionless temperature vs. the non-dimensional axial coordinate. The curves are visualized using the Eq. (3.3) for several values of the non-dimensional magnetic parameter (M) and in certain values held constant for other non-dimensional parameter.

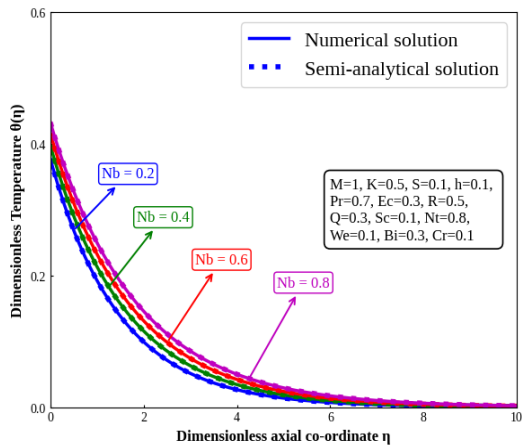


FIGURE 8. Dimensionless temperature in relation to non-dimensional axial coordinate. For specific values of the dimensionless Brownian motion factor (Nb) and for certain fixed values of the other non-dimensional parameters, the curves are plotted using Eq. (3.3).

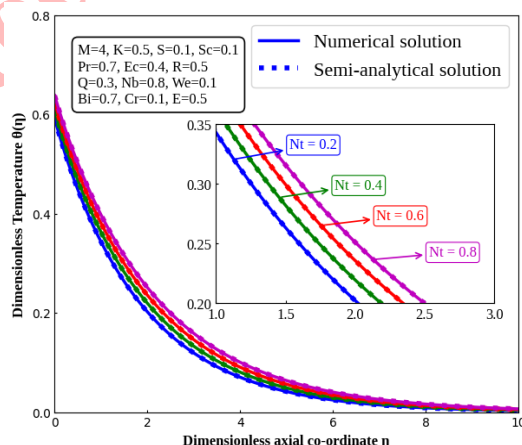


FIGURE 9. Plots of the non-dimensional temperature versus the dimensionless axial coordinate have been plotted using Eq. (3.3) for various values of the non-dimensional Thermophoresis factor (Nt), with some dimensionless parameters held at fixed values.



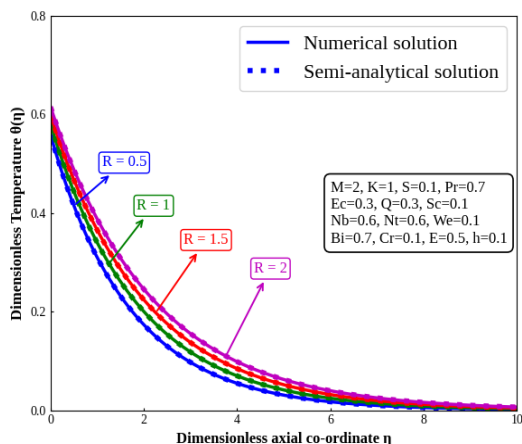


FIGURE 10. Plots of the non-dimensional temperature related to dimensionless axial coordinate have been generated using Eq. (3.3) for multiple values of the dimensionless Radiation (R), with other non-dimensional parameters are constant.

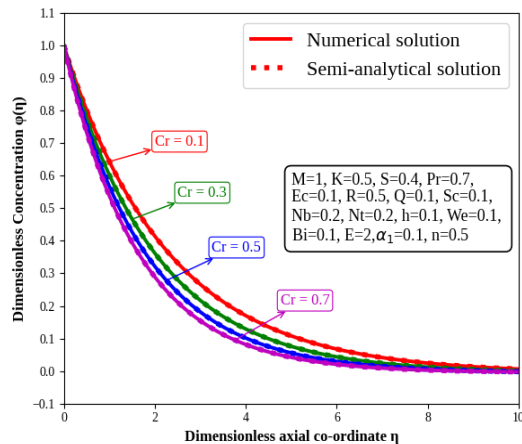


FIGURE 11. Dimensionless concentration versus the non-dimensional axial coordinate. The curves are visualized using the Eq. (3.4) for various values of the dimensionless Chemical reaction factor (Cr) and in specific fixed values of the other non-dimensional parameters.

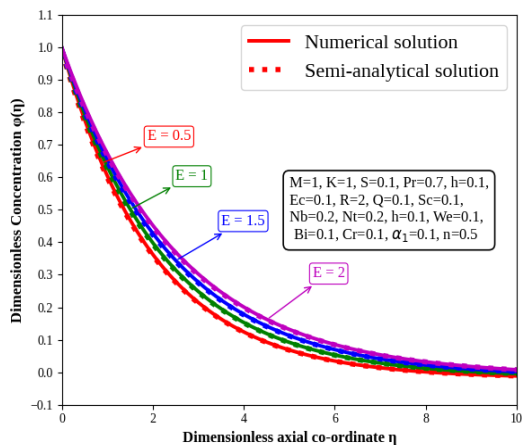


FIGURE 12. Dimensionless concentration against non-dimensional axial coordinate. The curves are plotted according to Eq. (3.4) for several values of the non-dimensional activation energy factor (E) and in some dimensionless parameters held at constant.

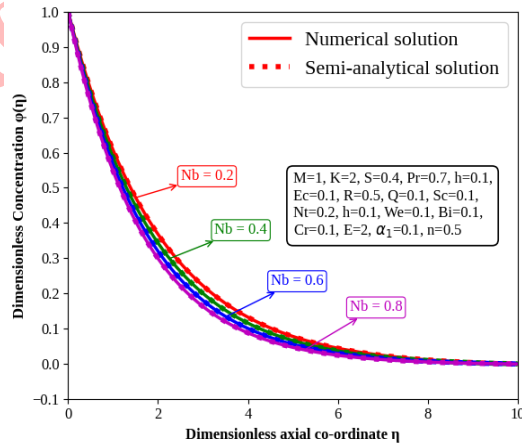


FIGURE 13. Non-dimensional concentration in relation to the dimensionless axial coordinate. Several values of the non-dimensional Brownian motion factor (Nb) and for particular fixed values of the other non-dimensional parameters, the curves are plotted using Eq. (3.4).

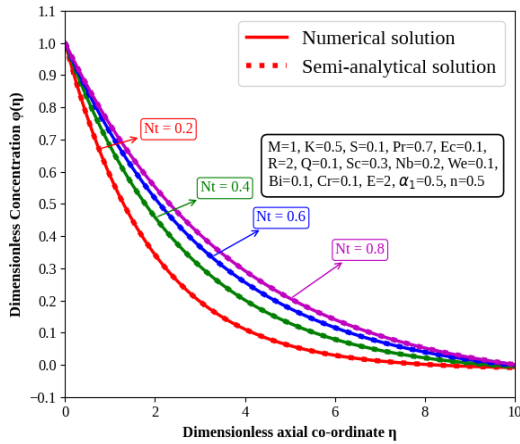


FIGURE 14. Plots of the non-dimensional concentration vs. the dimensionless axial coordinate have been plotted using Eq. (3.4) for various values of the dimensionless Thermophoresis factor (Nt), with other parameters are fixed.

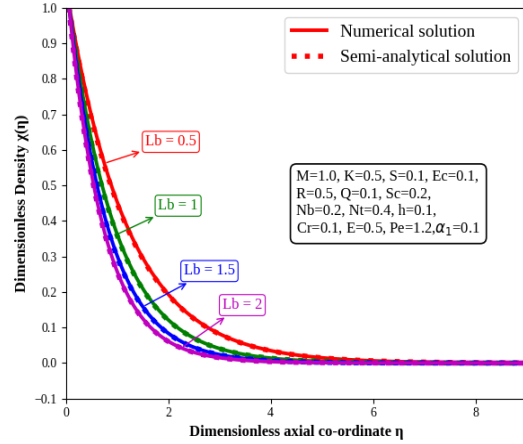


FIGURE 15. Non-dimensional density related to the dimensionless axial coordinate. The graphs are plots based on Eq. (3.5) for a range values of the non-dimensional Bioconvection Lewis number (Lb) and in particular dimensionless parameters are fixed.

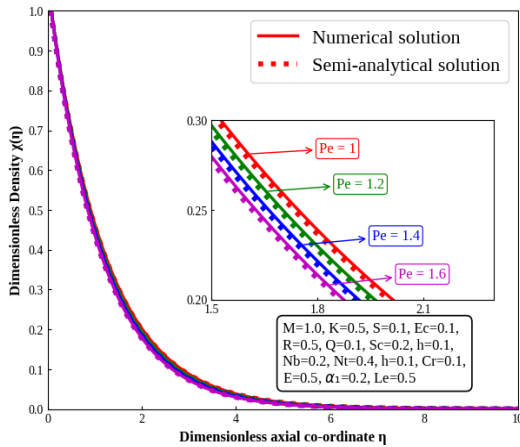


FIGURE 16. Dimensionless density versus non-dimension axial coordinate. For several values of the dimensionless Peclet number (Pe) and for some non-dimensional parameters held constant, the curves are plotted using Eq. (3.5).

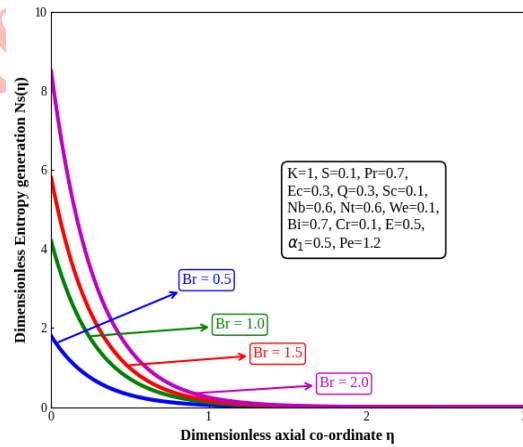


FIGURE 17. Non-dimensional entropy generation versus the dimensionless axial coordinate over a range of values for the non-dimensional Brinkman number (Br) at dimensionless parameters keep constant, as per Eq. (2.15).



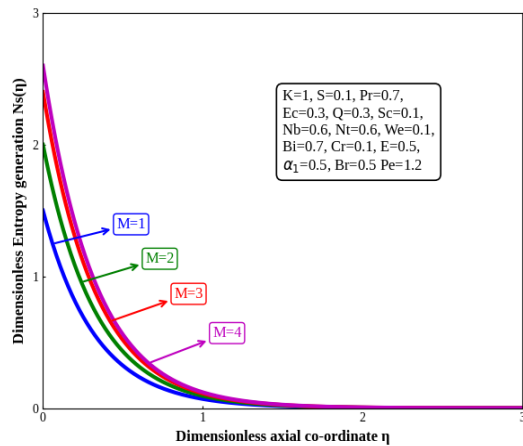


FIGURE 18. Dimensionless entropy generation vs. the non-dimensional axial coordinate for several values of the non-dimensional magnetic parameter (M) at some dimensionless parameters held at fixed values, as per Eq. (2.15).

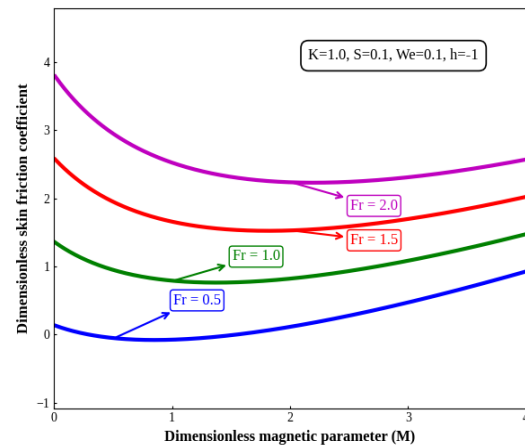


FIGURE 19. Non-dimensional skin friction related to dimensionless magnetic (M) for a range of values of the non-dimensional Forchheimer inertia factor (Fr) at other non-dimensional parameters are fixed, as per Eq. (3.12).

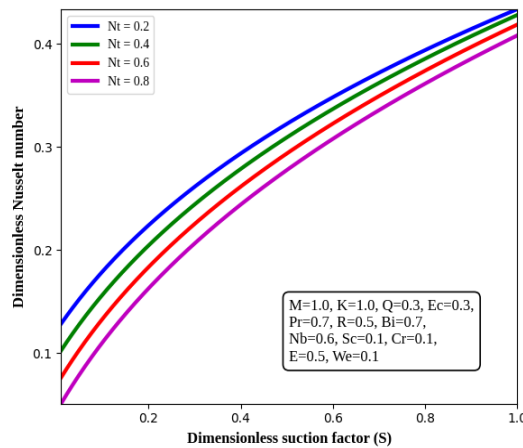


FIGURE 20. Dimensionless Nusselt number vs. the non-dimension suction factor (S) for multiple values of the dimensionless Thermophoresis parameter (Nt) at other non-dimensional parameters held constant, as per Eq. (3.13).

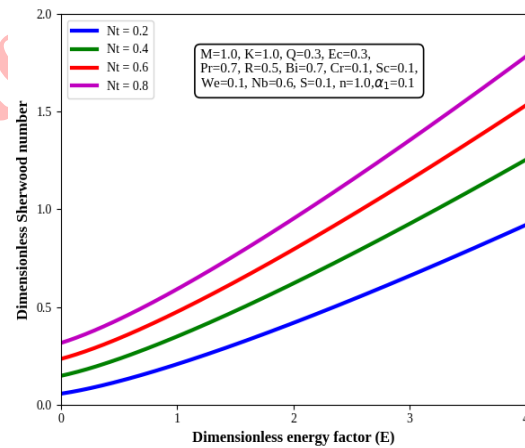


FIGURE 21. Non-dimensional Sherwood number, against the dimensionless energy factor (E) for several values of the non-dimensional Thermophoresis parameter (Nt) at other dimensionless parameters are fixed, as per Eq. (3.14).



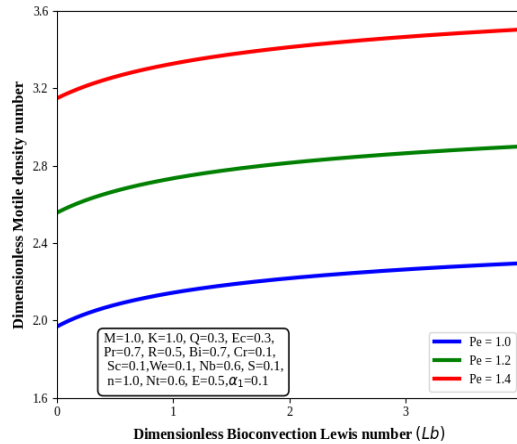


FIGURE 22. Dimensionless Motile density number, versus the non-dimension Bioconvection Lewis number (Lb) for different values of the dimensionless Peclet number (Pe) at other non-dimensional parameters held at fixed values, as per Eq. (3.15).

TABLE 2. Comparison of Numerical and Semi-analytical results for $(Re_x)^{-1/2}Nu$.

Pr	R	Q	Ec	Nb	Nt	S	Bi	Numerical solution	Semi-analytical solution	Error%
0.7	0.5	0.1	0.1	0.2	0.2	0.1	0.1	0.200651	0.215622	0.069432
0.8	0.5	0.1	0.1	0.2	0.2	0.1	0.1	0.209637	0.218272	0.039561
0.9	0.5	0.1	0.1	0.2	0.2	0.1	0.1	0.217624	0.220921	0.014924
0.7	0.5	0.1	0.1	0.2	0.2	0.1	0.1	0.214126	0.215622	0.006938
0.7	1.0	0.1	0.1	0.2	0.2	0.1	0.1	0.268170	0.204000	0.314559
0.7	1.5	0.1	0.1	0.2	0.2	0.1	0.1	0.319090	0.193031	0.653051
0.7	0.5	0.1	0.1	0.2	0.2	0.1	0.1	0.168289	0.215622	0.219518
0.7	0.5	0.2	0.1	0.2	0.2	0.1	0.1	0.186183	0.210758	0.116603
0.7	0.5	0.3	0.1	0.2	0.2	0.1	0.1	0.202533	0.206531	0.019358
0.7	0.5	0.1	0.1	0.2	0.2	0.1	0.1	0.202533	0.215622	0.060703
0.7	0.5	0.1	0.2	0.2	0.2	0.1	0.1	0.157159	0.210377	0.252965
0.7	0.5	0.1	0.3	0.2	0.2	0.1	0.1	0.111471	0.205131	0.456586
0.7	0.5	0.1	0.1	0.2	0.2	0.1	0.1	0.210720	0.215622	0.022734
0.7	0.5	0.1	0.1	0.4	0.2	0.1	0.1	0.205288	0.196377	0.045377
0.7	0.5	0.1	0.1	0.6	0.2	0.1	0.1	0.198752	0.178489	0.119128
0.7	0.5	0.1	0.1	0.2	0.2	0.1	0.1	0.205598	0.215622	0.046489
0.7	0.5	0.1	0.1	0.2	0.4	0.1	0.1	0.203600	0.196377	0.036781
0.7	0.5	0.1	0.1	0.2	0.6	0.1	0.1	0.201454	0.178489	0.128663
0.7	0.5	0.1	0.1	0.2	0.2	0.1	0.1	0.202533	0.215622	0.060703
0.7	0.5	0.1	0.1	0.2	0.2	0.2	0.1	0.215301	0.206377	0.043241
0.7	0.5	0.1	0.1	0.2	0.2	0.3	0.1	0.227063	0.197754	0.148209
0.7	0.5	0.1	0.1	0.2	0.2	0.1	0.1	0.098279	0.215622	0.544207
0.7	0.5	0.1	0.1	0.2	0.2	0.1	0.2	0.202533	0.226244	0.104803
0.7	0.5	0.1	0.1	0.2	0.2	0.1	0.3	0.256363	0.236865	0.082317
Absolute Average Error Percentage										0.150285



TABLE 3. Comparison of Numerical and Semi-analytical results for $Sh/\sqrt{Re_x}$.

Sc	Cr	Nb	Nt	E	Numerical solution	Semi-analytical solution	Error%
0.1	0.1	0.2	0.6	0.5	0.081285	0.134186	0.394237
0.3	0.1	0.2	0.6	0.5	0.20454	0.357390	0.427684
0.5	0.1	0.2	0.6	0.5	0.319531	0.471219	0.321906
0.1	0.1	0.2	0.6	0.5	0.20454	0.193505	0.057026
0.1	0.3	0.2	0.6	0.5	0.331816	0.234355	0.415870
0.1	0.5	0.2	0.6	0.5	0.425054	0.270577	0.570917
0.1	0.1	0.2	0.6	0.5	0.080851	0.193505	0.582177
0.1	0.1	0.4	0.6	0.5	0.183881	0.259689	0.291919
0.1	0.1	0.6	0.6	0.5	0.218341	0.295192	0.260343
0.1	0.1	0.2	0.2	0.5	0.246190	0.451593	0.454840
0.1	0.1	0.2	0.4	0.5	0.218072	0.280860	0.223555
0.1	0.1	0.2	0.6	0.5	0.191366	0.193505	0.011055
0.1	0.1	0.2	0.6	0.5	0.178927	0.193505	0.075338
0.1	0.1	0.2	0.6	1.0	0.156203	0.169915	0.080700
0.1	0.1	0.2	0.6	1.5	0.141155	0.193505	0.270536
Average Error Percentage							0.295874

TABLE 4. Comparison of Numerical and Semi-analytical results for $Nh/\sqrt{Re_x}$.

Le	Pe	δ_1	Numerical solution	Semi-analytical solution	Error%
0.5	1.0	0.2	0.433115	0.804853	0.461870
1.0	1.0	0.2	0.645337	1.102367	0.414590
1.5	1.0	0.2	0.838304	1.147917	0.269717
0.5	1.0	0.2	0.679127	0.848527	0.199640
0.5	1.2	0.2	0.712947	0.870103	0.180618
0.5	1.4	0.2	0.746807	0.891000	0.161833
0.5	1.0	0.2	0.645337	0.848527	0.239462
0.5	1.0	0.4	0.665762	0.963393	0.308940
0.5	1.0	0.6	0.686187	1.066646	0.356687
Absolute Average Error percentage					0.288151

5. CONCLUSION

This research effectively used both Homotopy analysis method (HAM) as well as Modified Homotopy analysis method (MHAM) to compute analytical approximations for unit less axial velocity, temperature, concentration and density. The graphical displays of several parameters on velocity, density, temperature, concentration, and entropy generation provided a good grasp of the system's behavior. The assessment of semi-analytical results to numerical results demonstrated high consistency, determining the accuracy and effectiveness of both HAM and MHAM approaches. These results contribute to a good understanding of the core physical phenomena and can be useful for optimizing system performance and better efficiency. The principal observations can be summarized as:

- An augment in the Brinkman number(Br) yields greater entropy generation due to intensified viscous dissipation, which converts more mechanical energy into heat. The density number fall with elevate values of the Bioconvection constant (δ_1) also Lb, Pe .
- Velocity increases with decline the parameter Forchheimer inertia factor (Fr), suction(S), K, M . Increasing the temperature difference factor (L_1), K and M outcomes in increased entropy generation.



- The thermal curve is strengthens with rising Eckert number (Ec), radiation parameter (R), thermophoresis factor (Nt), Nb , and Bi . The motile density number goes up with the Lb , Pe also δ_1 .
- The suction(S) exhibits an inverse trend, reducing the thermal curve. The Peclet number (Pe), radiation (R), heat source parameter (Q), suction (S) and Biot number (Bi) noticeably increase thermal efficiency near the surface.
- Increasing the activation energy parameter raises the concentration curve. The solutal transfer rate near the surface increases with higher values of Brownian motion term (Nb), Sc , Cr , but decreases with higher thermophoresis factor (Nt) and activation energy (E).

Future research could investigate three-dimensional and unsteady effects on Williamson bioconvective nanofluid flow, investigate non-Newtonian models with unique rheological characteristics in porous media, and leverage machine learning approaches to optimize entropy generation analysis, thereby providing further insights and improvements.

APPENDIX

Appendix A: Approximate analytical expressions for non - linear differential Eq. (2.8) via Homotopy analysis method

This appendix provides the detailed derivation of semi-analytical solution (3.1) for the given problem through Homotopy analysis method. We construct as following homotopy for Eq. (2.8):

$$(1-p)(f''' - (M+K)f') = hp((1+We f'')f''' - (M+K)f' + ff'' - Fr f'^2 - f'^2). \quad (\text{A. 1})$$

The initial approximation for Eq. (A. 1) is provided by

$$f_o(0) = S, f'_o(0) = 1, f'_o(\infty) = 0, \quad (\text{A. 2})$$

$$f_i(0) = 0, f'_i(0) = 0, f_i(\infty) \rightarrow 0, i = 1, 2, 3, \dots \quad (\text{A. 3})$$

Homotopy Eq. (A. 1) can be rewrite as:

$$\begin{aligned} (1-p) & \left\{ (f_0 + pf_1 + p^2 f_2 + \dots)''' - (M+K)(f_0 + pf_1 + p^2 f_2 + \dots)' \right\} \\ & = hp \left\{ (1+We)(f_0 + pf_1 + p^2 f_2 + \dots)''' (f_0 + pf_1 + p^2 f_2 + \dots)' \right. \\ & \quad - (M+K)(f_0 + pf_1 + p^2 f_2 + \dots)' \\ & \quad + (f_0 + pf_1 + p^2 f_2 + \dots)(f_0 + pf_1 + p^2 f_2 + \dots)'' \\ & \quad \left. - Fr [(f_0 + pf_1 + p^2 f_2 + \dots)']^2 - [(f_0 + pf_1 + p^2 f_2 + \dots)']^2 \right\}, \end{aligned} \quad (\text{A. 4})$$

Here,

$$f = f_o + pf_1 + p^2 f_2 + \dots \quad (\text{A. 5})$$

Equating constant terms in Eq. (A. 3), we get

$$f_o''' - (M+K)f'_o = 0. \quad (\text{A. 6})$$

Applying the boundary conditions given in Eq. (A. 2), we determine the value of f_0

$$f_o(\eta) = S + \frac{1}{\sqrt{M+K}} - \frac{e^{-\sqrt{M+K}\eta}}{\sqrt{M+K}}, \quad (\text{A. 7})$$

$$f'_o(\eta) = e^{-\sqrt{M+K}\eta}. \quad (\text{A. 8})$$

Equating coefficient of p terms in Eq. (A. 4), we get

$$f_1''' - (M+K)f'_1 - f_o''' - (M+K)f'_o = h((1+We f_o'')f_o''' - (M+K)f'_o + f_o f_o'' - Fr f_o'^2 - f_o'^2). \quad (\text{A. 9})$$



Applying the boundary specifications Eq. (A. 3), we determine the expression for f_1

$$f_1 = \left(\begin{aligned} & \frac{1}{6} \cdot \frac{We\sqrt[3]{M+K} + 7Fr}{\sqrt[3]{M+K}} + \frac{1}{2} \cdot \frac{1 + 10S\sqrt{M+K}}{\sqrt[3]{M+K}} \\ & + \left(-\frac{1}{2} \cdot \frac{1 + 10S\sqrt{M+K}}{\sqrt[3]{M+K}} - \frac{1}{3} \cdot \frac{We\sqrt[3]{M+K} + 7Fr}{\sqrt[3]{M+K}} \right) e^{-\sqrt{M+K} \eta} \\ & - \frac{1}{2} \cdot \frac{1 + 10S\sqrt{M+K}}{M+K} \cdot \eta e^{-\sqrt{M+K} \eta} \\ & + \frac{1}{6} \cdot \frac{(We\sqrt[3]{M+K} + 7Fr) e^{-2\sqrt{M+K} \eta}}{\sqrt[3]{M+K}} \end{aligned} \right). \tag{A. 10}$$

The HAM technique yields,

$$f = \lim_{p \rightarrow 1} f(\eta) = f_o + f_1. \tag{A. 11}$$

Hence, the semi-analytical solutions of the velocity distribution, is obtained by substituting the Eqs. (A. 7) and (A. 10) into the Eq. (A. 11), as follows

$$f(\eta) = S + \frac{1}{\sqrt{M+K}} - \frac{e^{-\sqrt{M+K} \eta}}{\sqrt{M+K}} + h \left[\begin{aligned} & \frac{1}{6} \cdot \frac{We\sqrt[3]{M+K} + 7Fr}{\sqrt[3]{M+K}} + \frac{1}{2} \cdot \frac{1 + 10S\sqrt{M+K}}{\sqrt[3]{M+K}} \\ & + \left(-\frac{1}{2} \cdot \frac{1 + 10S\sqrt{M+K}}{\sqrt[3]{M+K}} - \frac{1}{3} \cdot \frac{We\sqrt[3]{M+K} + 7Fr}{\sqrt[3]{M+K}} \right) e^{-\sqrt{M+K} \eta} \\ & - \frac{1}{2} \cdot \frac{1 + 10S\sqrt{M+K}}{M+K} \cdot \eta e^{-\sqrt{M+K} \eta} \\ & + \frac{1}{6} \cdot \frac{(We\sqrt[3]{M+K} + 7Fr) e^{-2\sqrt{M+K} \eta}}{\sqrt[3]{M+K}} \end{aligned} \right]. \tag{A. 12}$$

Appendix B: Semi-analytical expressions for the non - linear differential Eqs. (2.9)-(2.11) via Modified Homotopy analysis method (MHAM). This appendix outline the derivation of semi-analytical expressions of Eqs. (3.3)-(3.5) using MHAM method, which can be obtained by rewriting Eqs. (2.9) to (2.11) in a suitable form,

$$\left(1 + \frac{4}{3}R \right) \theta'' + Pr \left[f\theta' + Nb\theta'\phi' + Nt\theta'^2 + MEcf'^2 + Ecf''^2 + \frac{1}{\sqrt{2}}EcWe f''^3 + Q\theta \right] = 0, \tag{B. 1}$$

$$\phi'' + Scf\phi' + \left(\frac{Nt}{Nb} \right) \theta'' - ScCr(1 + \alpha_1\theta)^n \exp \left(\frac{-E}{1 + \alpha_1\theta} \right) \phi = 0, \tag{B. 2}$$

$$\chi'' + Lbf\chi' - Pe[(\delta_1 + \chi)\phi'' + \chi'\phi'] = 0. \tag{B. 3}$$

Now, we generate the following Homotopy for the Eqs. (B. 1)-(B. 3) as follows

$$(1-p) \left(1 + \frac{4}{3}R \right) \theta'' = hp \left[\left(1 + \frac{4}{3}R \right) \theta'' + Pr \left[f\theta' + Nb\theta'\phi' + Nt\theta'^2 + MEcf'^2 + Ecf''^2 + \frac{1}{\sqrt{2}}EcWe f''^3 + Q\theta \right] \right], \tag{B. 4}$$

$$(1-p)\phi'' = hp \left(\phi'' + Scf\phi' + \left(\frac{Nt}{Nb} \right) \theta'' - ScCr(1 + \alpha_1\theta)^n \exp \left(\frac{-E}{1 + \alpha_1\theta} \right) \phi \right), \tag{B. 5}$$

$$(1-p)\chi'' = hp(\chi'' + Lbf\chi' - Pe[(\delta_1 + \chi)\phi'' + \chi'\phi']). \tag{B. 6}$$



Initial approximations for Eqs. (B. 4)-(B. 6) are given by

$$\theta'_o(0) = Bi(\theta_o(0) - 1), \theta_o(\infty) \rightarrow 0, \phi_o(0) = 1, \phi_o(\infty) \rightarrow 0 \text{ and } \chi_o(0) = 1, \chi_o(\infty) \rightarrow 0, \quad (\text{B. 7})$$

$$\left. \begin{aligned} \theta'_i(0) &= Bi(\theta_i(0)), \quad \theta_i(\infty) \rightarrow 0, \\ \phi_i(0) &= 0, \quad \phi_i(\infty) \rightarrow 0, \\ \chi_i(0) &= 0, \quad \chi_i(\infty) \rightarrow 0, \quad i = 1, 2, 3, \dots \end{aligned} \right\} \quad (\text{B. 8})$$

Approximate analytical solutions to the Eqs. (B. 4)-(B. 6) are:

$$\theta = \theta_o + p\theta_1 + p^2\theta_2 + \dots, \quad (\text{B. 9})$$

$$\phi = \phi_o + p\phi_1 + p^2\phi_2 + \dots, \quad (\text{B. 10})$$

$$\chi = \chi_o + p\chi_1 + p^2\chi_2 + \dots \quad (\text{B. 11})$$

Substituting the Eq. (B. 11) into the Eqs. (B. 4) to (B. 6) respectively and comparing the coefficients of like powers of p , we acquire the following equations

$$p^0 : \theta''_o = 0, \quad (\text{B. 12})$$

$$p^1 : \theta''_1 - \theta''_o = h \left[\left(1 + \frac{4}{3}R\right) \theta''_o + Pr \left[f_o \theta'_o + Nb \theta'_o \phi'_o + Nt \theta_o'^2 + MEc f_o'^2 + Ec f_o''^2 + \frac{1}{\sqrt{2}} Ec W e f_o''^3 + Q \theta_o \right] \right], \quad (\text{B. 13})$$

$$p^0 : \phi''_o = 0, \quad (\text{B. 14})$$

$$p^1 : \phi''_1 - \phi''_o = h \left(\phi''_o + Sc f_o \phi'_o + \left(\frac{Nt}{Nb}\right) \theta''_o - Sc Cr (1 + \alpha_1 \theta_o)^n \exp\left(\frac{-E}{1 + \alpha_1 \theta_o}\right) \phi_o \right), \quad (\text{B. 15})$$

$$p^0 : \chi''_o = 0, \quad (\text{B. 16})$$

$$p^1 : \chi''_1 - \chi''_o = h(\chi''_o + Lb f_o \chi'_o - Pe[(\delta_1 + \chi_o) \phi''_o + \chi'_o \phi'_o]). \quad (\text{B. 17})$$

The initial guessing solutions for the Eqs. (B. 4) to (B. 6) are constructed using MHAM, which satisfies the boundary conditions in Eq. (B. 7) are:

$$\theta_o(\eta) = \frac{Bi \times e\left(-\sqrt{\frac{Q+S}{MEcR+Nb+Nt}}\eta\right)}{\sqrt{\frac{Q+S}{MEcR+Nb+Nt}} + Bi}, \quad (\text{B. 18})$$

$$\phi_o(\eta) = e\left(-\sqrt{\frac{Sc+CrNb}{(R+E)Nt}}\eta\right), \quad (\text{B. 19})$$

$$\chi_o(\eta) = e\left(-\sqrt{Lb+Pe\alpha_1}\eta\right). \quad (\text{B. 20})$$

Utilizing the boundary conditions in Eq. (B. 11), we determine the Eqs. (B. 21)-(B. 23) are obtained by substituting the Eqs. (B. 13), (B. 15) and (B. 17) respectively, as follows

$$\theta_1(\eta) = h \left[\begin{array}{l} \frac{(MEcR + Nb + Nt)e^{(-A\eta)} Pr Bi C}{(Q + S)(A + Bi) \left(1 + \frac{4}{3}R\right)} \\ - \frac{1}{4} \frac{e^{(-2\sqrt{M+K}\eta)} Pr Ec (2M + K)}{(M + K) \left(1 + \frac{4}{3}R\right)} \\ - \frac{e^{-(A+\sqrt{M+K})\eta} Pr Bi A}{(A + \sqrt{M + K})^2 (A + Bi) \left(1 + \frac{4}{3}R\right) \sqrt{M + K}} \\ + \frac{1}{18} \frac{\sqrt{M + K} e^{(-3\sqrt{M+K}\eta)} Pr Ec W e \sqrt{2}}{\left(1 + \frac{4}{3}R\right)} \\ - \frac{1}{4} \frac{e^{(-2A\eta)} Pr Nt Bi^2}{(A + Bi)^2 \left(1 + \frac{4}{3}R\right)} + \frac{e^{-(A+B)\eta} Pr Nb Bi AB}{(A + B)^2 (A + Bi) \left(1 + \frac{4}{3}R\right)} \\ N_1 - Bi N_2 \end{array} \right] / Bi, \quad (\text{B. 21})$$



$$\begin{aligned}
 \phi_1(\eta) = h & \left[\frac{(E + R) Nt e^{-B\eta} \left(\left(S + \frac{1}{\sqrt{M+K}} \right) Sc B + Sc Cr - Sc Cr E \right)}{Sc + Cr Nb} \right. \\
 & - \frac{e^{-(\sqrt{M+K}-B)\eta} Sc B}{(\sqrt{M+K} + B)^2 \sqrt{M+K}} + \frac{Sc B}{(\sqrt{M+K} + B)^2 \sqrt{M+K}} \\
 & + \frac{e^{-(A+B)\eta} \left(\frac{Sc Cr E \alpha_1 Bi + Sc Cr n \alpha_1 Bi - E n \alpha_1 Bi}{A+Bi} \right)}{(A+B)^2} \\
 & + \frac{e^{-(2A+B)\eta} n E \alpha_1^2 Bi^2}{(2A+B)^2 (A+Bi)^2} + \frac{Nt Bi}{(A+Bi) Nb} - \frac{e^{-B\eta} Nt Bi}{(A+Bi) Nb} \\
 & - \frac{(E + R) Nt \left(\left(S + \frac{1}{\sqrt{M+K}} \right) Sc B + Sc Cr - Sc Cr E \right)}{Sc + Cr Nb} \\
 & \left. - \left(\frac{Sc Cr E \alpha_1 Bi + Sc Cr n \alpha_1 Bi - E n \alpha_1 Bi}{(A+Bi)(A+B)^2} \right) - \frac{n E \alpha_1^2 Bi^2}{(2A+B)^2 (A+Bi)^2} \right], \tag{B. 22}
 \end{aligned}$$

$$\begin{aligned}
 \chi_1(\eta) = h & \left[\frac{e^{(-D\eta)} Lb \left(S + \frac{1}{\sqrt{M+K}} \right)}{\sqrt{Lb + Pe \alpha_1}} - \frac{e^{-(\sqrt{M+K}+D)\eta} Lb D}{(\sqrt{M+K} + D)^2 \sqrt{M+K}} \right. \\
 & \left. - \frac{(E + R) Nt e^{(-B\eta)} Pe \alpha_1}{Sc + Cr Nb} + \frac{e^{-(B+D)\eta} \left(\frac{Pe(Sc+CrNb)}{(R+E)Nt} - Pe DB \right)}{(B+D)^2} \right]. \tag{B. 23}
 \end{aligned}$$

Based on the Homotopy analysis method (HAM) technique, we have

$$\begin{aligned}
 \theta &= \lim_{p \rightarrow 1} \theta(\eta) = \theta_o + \theta_1, \\
 \phi &= \lim_{p \rightarrow 1} \phi(\eta) = \phi_o + \phi_1, \\
 \chi &= \lim_{p \rightarrow 1} \chi(\eta) = \chi_o + \chi_1.
 \end{aligned} \tag{B. 24}$$

Hence, the semi-analytical solutions of the temperature, concentration, and density distribution equations result from substituting the Eq. (B. 18) to (B. 20) and (B. 21) to (B. 23) into the Eq. (B. 24) respectively, which are given in the text Eqs. (3.3)-(3.5) and the constants are defined in (3.6)-(3.11).

Appendix C: Nomenclature.

Symbol	Meaning
Bi	Biot number
B_o	Uniform magnetic field (kg / S ² A)
D_B	Brownian diffusion coefficient
η	Dimensionless axial co-ordinate
$f'(\eta)$	Dimensionless velocity
Cr	Chemical reaction parameter
Ec	Eckert number
D_T	Thermophoresis diffusion coefficient
$\theta(\eta)$	Dimensionless temperature
K_c	Rate of reaction constant
Fr	Darcy Forchheimer
K	Porosity parameter



M	Magnetic field
$\phi(\eta)$	Dimensionless concentration
Lb	Bioconvection Lewis number
Nt	Thermophoresis parameter
$\chi(\eta)$	Dimensionless density
Br	Brinkman number
C_f	Skin friction coefficient
Nu	Nusslet number
Nh	Motile micro organism density number
Nb	Brownian motion
Sh	Sherwood number
Pr	Prandtl number
Sc	Schmidt number
Pe	Peclet number
R	Radiation parameter
Q	Heat source parameter
S	Suction parameter
u, v	Velocity components in x and y directions (m/s)
T_∞	Free stream temperature(K)
δ_1	Bioconvection constant
We	Williamson fluid parameter
x, y	Cartesian coordinates (m)
ρ	Fluid density (kg/m^3)
ν	Kinematic viscosity (m^2/s)
ρC_p	Fluid thermal capacity (J/m^3K)
μ	Dynamic viscosity ($kg/(ms)$)

CONFLICT OF INTERESTS

The authors declare that there is no conflict of interests.

ACKNOWLEDGMENT

The authors are very grateful to the reviewers for carefully reading the paper and for their comments and suggestions which have improved the paper. Also, the authors are thankful to Sri. S. Natanagopal, Secretary, The Madura College Board, Dr. J. Suresh, The Principal, The Madura College and Dr. C. Thangapandi, Head of the Department, The Madura College, Madurai, Tamil Nadu, India for their constant support to our research work.

REFERENCES

- [1] B. Ahmad, M. Idrees, S. A. A. Shah, K. S. Nisar, and A. H. Abdel-Aty, *A study on the impact of solar radiations and activation energy effects in existence of nanofluid over stretching solar sheets*, Case Stud. Therm. Eng., 59 (2024), 104448.
- [2] F. Ali, A. Zaib, T. Padmavathi, M. Faizan, and S. S. Zafar, *Exact solution of radiative flow on the mixed convection flow of hybrid nanofluid in a porous medium: Laplace transform technique for sustainable energy*, Surf. Rev. Lett., (2025), 2550116.
- [3] A. U. Awan, S. A. A. Shah, and B. Ali, *Bio-convection effects on Williamson nanofluid flow with exponential heat source and motile microorganism over a stretching sheet*, Chin. J. Phys., 77 (2022), 2795–2810.



- [4] U. Adnan, N. Ahmed, S. T. Mohyud-Din, M. D. Alsulami, and I. Khan, *A novel analysis of heat transfer in the nanofluid composed by nanodiamond and silver nanomaterials: numerical investigation*, *Sci. Rep.*, *12*(1) (2022), 1284.
- [5] R. P. Agarwal, A. M. Alghamdi, S. Gala, and M. A. Ragusa, *On the regularity for weak solutions to the micropolar fluid flows*, *Applied and Computational Mathematics*, *23*(4) (2024), 558-569.
- [6] S. U. R. K. Akbarov, G. J. Valiyev, S. A. Aliyev, and Z. F. Khankishiyev, *The influence of the inhomogeneous initial stresses in the hollow cylinder containing an inviscid fluid on the dispersion of the quasi-Scholte waves propagating in this cylinder*, *Applied and Computational Mathematics*, *23*(1) (2024).
- [7] V. Ananthaswamy, T. Nithya, and V. K. Santhi, *Approximate analytical expressions of a boundary layer flow of viscous fluid using the modified Homotopy analysis method*, *J. Inf. Comput. Sci.*, *9*(8) (2019), 534-541.
- [8] V. Ananthaswamy and L. S. Amalraj, *Thermal stability analysis of reactive hydromagnetic third-grade fluid using Homotopy analysis method*, *Int. J. Mod. Math. Sci.*, *14*(1) (2016), 25-41.
- [9] V. Ananthaswamy, C. Sumathi, and M. Subha, *Mathematical analysis of variable viscosity fluid flow through a channel and Homotopy Analysis Method*, *Int. J. Mod. Math. Sci.*, *14*(3) (2016), 296-316.
- [10] V. Ananthaswamy, B. Seethalakshmi, and V. Santhi, *Approximate analytical solutions for chemical entropy generation and MHD effects on the unsteady heat and fluid flow through a porous medium using modified homotopy analysis method*, (2022).
- [11] V. Ananthaswamy, C. Sumathi, and V. K. Shanthi, *A mathematical study on MHD boundary layer flow of nanofluid and heat transfer over a porous exponentially stretching sheet*, *Adv. Math. Sci. J.*, *8* (2019), 109-130.
- [12] M. I. Asjad, M. Zahid, M. Inc, D. Baleanu, and B. Almohsen, *Impact of activation energy and MHD on Williamson fluid flow in the presence of bioconvection*, *Alex. Eng. J.*, *61*(11) (2022), 8715-8727.
- [13] S. Baag, S. R. Mishra, G. C. Dash, and M. R. Acharya, *Entropy generation analysis for viscoelastic MHD flow over a stretching sheet embedded in a porous medium*, *Ain Shams Eng. J.*, *8*(4) (2017), 623-632.
- [14] A. S. Butt, A. Ali, and A. Mehmood, *Numerical investigation of magnetic field effects on entropy generation in viscous flow over a stretching cylinder embedded in a porous medium*, *Energy*, *99* (2016), 237-249.
- [15] W. Cao, S. U. Rehman, M. I. Asjad, and M. Inc, *Numerical study of bioconvection and Cattaneo-Christov heat flux model in MHD Maxwell nanofluid flow over a variable thickness elastic surface*, *Applied and Computational Mathematics*, *23*(2) (2024), 182-200.
- [16] S. U. Choi and J. A. Eastman, *Enhancing thermal conductivity of fluids with nanoparticles*, Argonne Natl. Lab. Rep. No. ANL/MSD/CP-84938; CONF-951135-29, Argonne, IL, 1995.
- [17] L. A. Dawood, M. Lakestani, and J. Manafian, *Breather wave solutions for the (3+ 1)-D generalized shallow water wave equation with variable coefficients*, *Qualitative Theory of Dynamical Systems*, *22*(4) (2023), 127.
- [18] M. Dhlamini, P. K. Kameswaran, P. Sibanda, S. Motsa, and H. Mondal, *Activation energy and binary chemical reaction effects in mixed convective nanofluid flow with convective boundary conditions*, *J. Comput. Des. Eng.*, *6*(2) (2019), 149-158.
- [19] M. Dhlamini, P. K. Kameswaran, P. Sibanda, S. Motsa, and H. Mondal, *Activation energy and binary chemical reaction effects in mixed convective nanofluid flow with convective boundary conditions*, *J. Comput. Des. Eng.*, *6*(2) (2019), 149-158.
- [20] F. Haq, S. Kadry, Y. M. Chu, M. Khan, and M. I. Khan, *Modeling and theoretical analysis of gyrotactic microorganisms in radiated nanomaterial Williamson fluid with activation energy*, *J. Mater. Res. Technol.*, *9*(5) (2020), 10468-10477.
- [21] A. Kumar, R. Tripathi, R. Singh, and V. K. Chaurasiya, *Simultaneous effects of nonlinear thermal radiation and Joule heating on the flow of Williamson nanofluid with entropy generation*, *Physica A*, *551* (2020), 123972.
- [22] G. Kumaran and N. Sandeep, *Thermophoresis and Brownian moment effects on parabolic flow of MHD Casson and Williamson fluids with cross diffusion*, *J. Mol. Liq.*, *233* (2017), 262-269.
- [23] M. Lakestani and J. Manafian, *Application of the ITEM for the modified dispersive water-wave system*, *Optical and Quantum Electronics*, *49*(4) (2017), 128.
- [24] C. G. Lakshmi, V. Ananthaswamy, and S. Sivasundaram, *Contribution of modified Homotopy analysis method on hydromagnetic layer of Casson fluid*, *Nonlinear Stud.*, *32*(1) (2025).



- [25] S. Liao, *Homotopy analysis method in nonlinear differential equations*, Vol. 153, Higher Education Press, Beijing, 2012.
- [26] S. Liao, *An optimal homotopy-analysis approach for strongly nonlinear differential equations*, Commun. Nonlinear Sci. Numer. Simul., *15*(8) (2010), 2003–2016.
- [27] S. Liao and A. Campo, *Analytic solutions of the temperature distribution in Blasius viscous flow problems*, J. Fluid Mech., *453* (2002), 411–425.
- [28] S. J. Liao, *An approximate solution technique not depending on small parameters: a special example*, Int. J. Non-Linear Mech., *30*(3) (1995), 371–380.
- [29] S. J. Liao, *Beyond Perturbation: Introduction to the Homotopy Analysis Method*, Chapman and Hall/CRC Press, Boca Raton, 2003.
- [30] S. J. Liao, *An explicit totally analytic approximation of Blasius viscous flow problems*, (1999), 75–78.
- [31] S. J. Liao, *On the analytic solution of magnetohydrodynamic flows of non-Newtonian fluids over a stretching sheet*, J. Fluid Mech., *488* (2003), 189–212.
- [32] A. Paul, J. Mani Nath, and T. Kanti Das, *An investigation of the MHD Cu-Al₂O₃/H₂O hybrid-nanofluid in a porous medium across a vertically stretching cylinder incorporating thermal stratification impact*, J. Therm. Eng., *9*(3) (2023).
- [33] M. V. Reddy, T. K. Das, K. Malleswari, J. M. Nath, S. Saroja, and V. M. Reddy, *MHD radiative Williamson nanofluid through Darcy–Forchheimer medium due to stretching sheet in the presence of heat source, activation energy and motile microorganisms*, Indian J. Chem. Technol., *32*(2) (2025), 176–189.
- [34] P. Sharma, N. Kumar, and T. Sharma, *Entropy analysis in MHD forced convective flow through a circular channel filled with porous medium in the presence of thermal radiation*, Int. J. Heat Technol., *34*(2) (2016), 311–318.
- [35] B. K. Sharma and R. Gandhi, *Combined effects of Joule heating and non-uniform heat source/sink on unsteady MHD mixed convective flow over a vertical stretching surface embedded in a Darcy-Forchheimer porous medium*, Propuls. Power Res., *11*(2) (2022), 276–292.
- [36] Y. Q. Song, S. U. Khan, M. I. Khan, M. Awais, A. Abbasi, and Q. H. Shi, *Bidirectional non-linear stretched flow of Williamson nanofluid with swimming of motile gyrotactic microorganisms*, Appl. Math. Comput., *411* (2021), 126502.
- [37] S. Sivasankari and V. Ananthaswamy, *A mathematical study on non-linear ordinary differential equation for Magnetohydrodynamic flow of the Darcy-Forchheimer nanofluid*, Comput. Methods Differ. Equ., *11*(4) (2023), 696–715.
- [38] R. Thenmozhi and V. Ananthaswamy, *Mathematical study on MHD fluid flow using homotopy analysis method*, AIP Conf. Proc., *2378*(1) (2021), 020018.
- [39] Z. Ullah, E. R. El-Zahar, M. S. Aldhabani, H. F. Alrihieli, and L. F. Seddek, *Heat transfer assessment with entropy generation and thermal density effects on boundary layer flow of magneto nanofluid across the stretching sheet under magnetic field*, Therm. Sci. Eng. Prog., *43* (2023), 101955.
- [40] K. Vijayalakshmi, A. Chandulal, H. Alhazmi, A. F. Aljohani, and I. Khan, *Effect of chemical reaction and activation energy on Riga plate embedded in a permeable medium over a Maxwell fluid flow*, Case Stud. Therm. Eng., *59* (2024), 104457.

